Arabian Journal of Chemistry (2022) **15**, 104381

King Saud University

Arabian Journal of Chemistry

www.ksu.edu.sa
www.sciencedirect.com

ORIGINAL ARTICLE

An indirect-to-direct band gap transition of $NaSbS_2$ via minor Ga doping: A theoretical study

Huan Peng [a], **Rongjian Sa** [b,*], **Diwen Liu** [a,*]

[a] *School of Materials and Chemical Engineering, Pingxiang University, Pingxiang 337055, China*
[b] *College of Materials and Chemical Engineering, Minjiang University, Fuzhou 350108, China*

Received 3 April 2022; accepted 19 October 2022
Available online 26 October 2022

KEYWORDS

$NaSbS_2$;
Ga doping;
Bandgap transition;
Optical property

Abstract The efficiency of $NaSbS_2$ is limited by its wide indirect band gap. Alloying is a very effective strategy to tune the band gap over a wide range for the mixed-anion $NaSb(S,Se)_2$ alloys. However, these compounds are still indirect band gap semiconductors. The influence of Ga doping on the structure, electronic, and optical properties of $NaSbS_2$ is studied for the first time. Our calculated results show that $NaSbS_2$ is an indirect band gap semiconductor, and the difference between the indirect and direct band gaps is less than 0.1 eV. Moreover, the forbidden transition is discovered for the fundamental direct bandgap of $NaSbS_2$. The results indicate that the $NaSb_{1-x}Ga_xS_2$ alloys are predicted to be synthesized in the proper conditions. An indirect-to-direct band gap transition is observed from $NaSbS_2$ to $NaSb_{1-x}Ga_xS_2$. The minor Ga doping (less than10 %) has little effect on the electronic and optical properties of $NaSbS_2$. Importantly, the weak transition of the fundamental direct bandgap is allowed for $NaSb_{1-x}Ga_xS_2$. This study can provide a route to explore the high efficiency of novel based-$NaSbS_2$ materials.

1. Introduction

Ternary metal chalcogenides with the formula of ABX_2 (A = Na, K, Cu, Ag; B = Sb, Bi; and X = S or Se) have attracted considerable interest because of their huge potential applications in photovoltaics. These compounds are non-toxic or less toxic, earth abundant, and inexpensive. The experimental band gaps of $NaBiS_2$ and $NaBiSe_2$ are in the ideal range (1.20–1.45 eV) and they show great of interest for applications in solar cells (Rosales et al., 2018). $KBiS_2$ and $KBiSe_2$ exhibit remarkable stability and strong optical absorption in the whole visible range.(Yang et al., 2019) The structure and optoelectronic properties of ternary metal chalcogenides $CuSb(S,Se)_2$ (Choi et al., 2015; Welch et al., 2015) and $Ag(Sb,Bi)S_2$ (Ho and Lee, 2013; Huang et al., 2013) have been studied in the past few years as the potential alternatives for applications in solar cells. High-throughput calculations for screening potential photovoltaic absorbers have been performed by computing the band gap and effective mass of carriers and 31 candidates are identified (Kang et al., 2019). Finally, taking earth abundance and low cost into account, three compounds $GeAs_2$, $SiAs_2$, and $NaSbS_2$ are considered as promising indirect bandgap semiconductors. In addition, the defect properties are studied in order to provide a guideline for optimizing growth conditions of these materials.

* Corresponding authors.
E-mail addresses: rjsa@mju.edu.cn (R. Sa), liudiwen1987@163.com (D. Liu).

Peer review under responsibility of King Saud University.

ELSEVIER Production and hosting by Elsevier

https://doi.org/10.1016/j.arabjc.2022.104381
1878-5352

$NaSbS_2$ is a kind of compound with the excellent properties of non-toxic, earth-abundant, and good stability. $NaSbS_2$ shows an optical band gap of 1.5–1.8 eV and high absorption coefficient (Bazakutsa et al., 1975; Rahayu et al., 2016). The initial efficiency of 3.18 % was achieved in 2016 for the first time (Rahayu et al., 2016). In 2018, the higher efficiency was 4.11 % for $NaSbS_2$. The structural, thermoelectric, electronic, and optical properties of $NaSbS_2$ and $NaSbSe_2$ have been investigated by using first-principles method (Dai et al., 2019; Khare et al., 2020; Mahmoud et al., 2019; Sun and Singh, 2017; Zhang et al., 2019). The recent theoretical study indicates that $NaSbS_2$ might be limited for solar cells due to the forbidden transition of fundamental direct bandgap (Leung et al., 2019). $NaSbSe_2$ has a narrower band gap of 1.48 eV and yields an efficiency of 2.22 % (Aragaw et al., 2017). The efficiency can be further improved by tuning the band gap of $NaSbS_2$ to the optimal bandgap (~1.4 eV) through adjusting the $NaSb(S,Se)_2$ alloy composition (Dai et al., 2019). Recently, the structural, mechanical, electronic, and optical properties of $Na_{1-x}Li_xSbS_2$ solid solutions have been performed (Liu et al., 2021). The results show that the suitable band gap of $NaSbS_2$ can be achieved by doping Li and applying moderate pressure. In addition, $NaSbX_2$ and $NaInX_2$ (X = S or Se) belong to the hexagonal (space group: *R*-3 *m*) and monoclinic (space group: *C*2/*c*) crystal structures, respectively (Hoppe et al., 1961; Olivier-Fourcade et al., 1978). Therefore, the compound $NaBX_2$ (X = S or Se) will undergo phase transition when Sb is replaced by In with a larger ion radius. The experimental and theoretical works have confirmed that $NaInX_2$ has a broader band gap than that of $NaSbX_2$ (Fukuzaki et al., 2000; Hossain et al., 2021b; Takahashi et al., 2018). The structural, elastic, and thermal properties of various $NaInS_{2-x}Se_x$ compounds have been explored in detail (Hossain et al., 2021a). Interestingly, three compounds $KInS_2$, $RbInS_2$, and $CsInS_2$ show the monoclinic crystal structures with space group *C*2/*c* (Eisenmann and Hofmann, 1991; Zeng et al., 2007), and they have larger direct band gaps (Bouchenafa et al., 2018).

The crystal structure and optical band gap of $NaGaS_2$ was studied by two research groups for the first time in 2020 (Adhikary et al., 2020; Klepov et al., 2020). $NaGaS_2$ is a monoclinic crystal structure with the *C*2/*c* space group and shows a wide optical band gap (~4.0 eV) (Adhikary et al., 2020). The recent theoretical calculations show that $NaGaS_2$ is a direct band gap compound (Yun et al., 2022). Our calculated results suggest that $NaSbS_2$ is a narrow indirect band gap semiconductor (Liu et al., 2021). Therefore, an indirect-to-direct band gap transition can be achieved from $NaSbS_2$ to $NaGaS_2$. Ga and Sb have similar ionic radii, so it is theoretically feasible to synthesize the $NaSb_{1-x}Ga_xS_2$ alloys. It should be pointed out that the doping Ga concentration must be controlled because high Ga doping concentration will lead to a significant increase in band gap of $NaSbS_2$. Here, the influence of Ga doping on the structure, electronic and optical properties of $NaSbS_2$ is reported based on first-principles calculations. It is discovered that the Ga minor doping is an effective strategy to obtain the direct band gap of highly stable $NaSbS_2$. The low concentration Ga doping has little effect on the electronic and optical properties of $NaSbS_2$. Moreover, the weak transition is allowed for the fundamental direct bandgap of $NaSb_{1-x}Ga_xS_2$. The present study can inspire experiment research to explore more novel based-$NaSbS_2$ materials with high efficiency.

2. Computational details

All the calculations were carried out via density functional theory (DFT), which was implemented in Vienna ab initio simulation package (VASP) (Kresse and Furthmüller, 1996). The generalized gradient approximation of Perdew-Burke-Ernzerhof (GGA-PBE) (Perdew et al., 1996) was used to deal with the exchange–correlation effects. The interactions between ions and electrons were described by the projector-augmented wave (PAW) (Blöchl, 1994) method with an energy cutoff of 350 eV. The valence electron configurations for Na, Sb, Ga, and S were $2p^63s^1$, $5s^25p^3$, $4s^24p^1$, and $3s^23p^4$, respectively. The geometry optimization convergence criteria were set to 1.0×10^{-5} eV and 0.01 eV/Å for total energy and the force on each atom, respectively. A $6 \times 6 \times 6$ *k*-point mesh was employed for $NaSbS_2$ and $NaSb_{0.75}Ga_{0.25}S_2$. $3 \times 3 \times 3$, $6 \times 3 \times 3$, and $6 \times 6 \times 3$ *k*-point meshes were selected for $NaSb_{1-x}Ga_xS_2$ with three doping concentrations of $\times$ = 0.03125, 0.0625, and 0.125, respectively.

3. Results and discussions

3.1. Structural properties

The monoclinic phase with space group *C*2/*c* of $NaSbS_2$ is chosen as the object of this study. The crystal structure of $NaSbS_2$ is depicted in Fig. 1. The calculated lattice constants of $NaSbS_2$ are a = 8.24 Å, b = 8.40 Å, and c = 6.91 Å, which are in good agreement with the experimental data (Olivier-Fourcade et al., 1978). In order to explore the impact of Ga doping on the physical properties of $NaSbS_2$, different supercells are modeled. The doping concentration is related to supercell size. There are four formula units (16 atoms) for the pristine $NaSbS_2$, so the $NaSb_{0.75}Ga_{0.25}S_2$ compound is simulated by substituting one Ga atom for one Sb atom. Accordingly, the $NaSb_{1-x}Ga_xS_2$ (x = 0.03215, 0.0625, and 0.125) compounds are simulated by $2 \times 2 \times 2$, $1 \times 2 \times 2$, and $1 \times 1 \times 2$ supercells when one Sb atom is replaced by one Ga atom. The local structural variation of $NaSbS_2$ is caused by the introduction of Ga atoms. For instance, the bond length is significantly shortened from Sb − S to Ga − S due to the smaller ionic radius of Ga^{3+}. According to our recent theoretical study (Sa et al., 2022), $NaSbS_2$ exhibits high stability. The thermodynamic stability of compound can be evaluated by calculating the formation enthalpy (ΔH). The stability of $NaSb_{1-x}Ga_xS_2$ is assessed in the present work by the following equation:

$$\Delta H(NaSb_{1-x}Ga_xS_2) = E(NaSb_{1-x}Ga_xS_2) + E(Sb) - E(NaSbS_2) - E(Ga) \quad (1)$$

where $E(NaSb_{1-x}Ga_xS_2)$, $E(NaSbS_2)$, $E(Sb)$ and $E(Ga)$ refer to the total energies of compounds and the energies of solid state Sb and Ga atoms, respectively. The calculated ΔH value of $NaSb_{1-x}Ga_xS_2$ is displayed in Fig. 2. The negative ΔH value confirms the stability of $NaSb_{1-x}Ga_xS_2$. It can be seen that

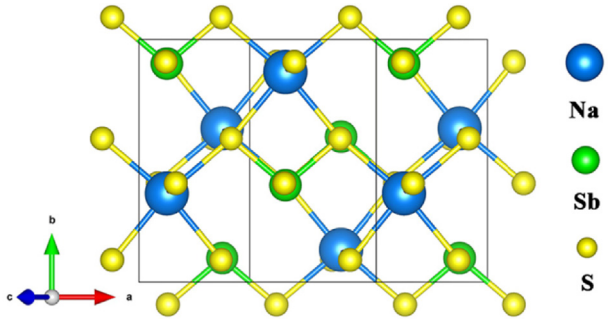

Fig. 1 Crystal structure of $NaSbS_2$.

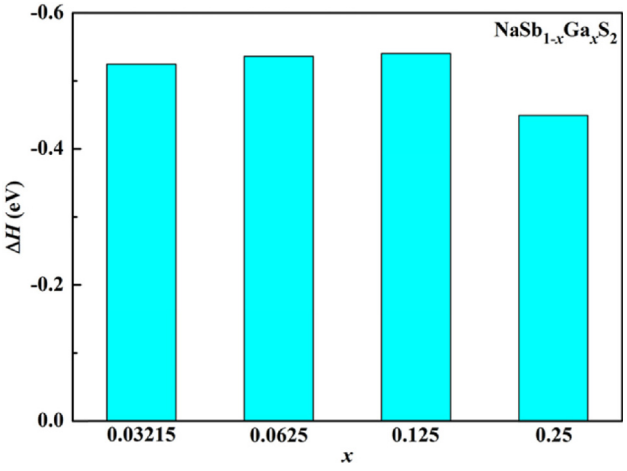

Fig. 2 The formation energies of the $NaSb_{1-x}Ga_xS_2$ compounds.

there is no difference in the stability of $NaSbS_2$ with low concentration Ga doping. Moreover, the stability of $NaSbS_2$ is slightly reduced when the concentration of Ga doping is high.

3.2. Electronic structure

The band structure and density of states of $NaSbS_2$ are analyzed, as shown in Fig. 3. The indirect band gap nature of $NaSbS_2$ is observed because the valence band maximum (VBM) and conduction band minimum (CBM) are located at the high symmetry Z and τ points, respectively. Several theoretical reports suggest that $NaSbS_2$ is an indirect band gap material (Kang et al., 2019; Mahmoud et al., 2019; Sun and Singh, 2017; Xia et al., 2017), while another theoretical study describes this compound to have a fundamental direct band gap (Leung et al., 2019). The indirect and direct band gaps are 0.88 and 0.98 eV for $NaSbS_2$, which is much smaller than the previous experimental data (Leung et al., 2019; Rahayu et al., 2016). The energy difference between the indirect and direct band gaps is small (only 0.1 eV). It is well known that the GGA-PBE method usually underestimates the band gap of semiconductor material. More accurate band gap can be obtained for $NaSbS_2$ from hybrid functional HSE06 (Liu et al., 2021). The band gap variation trend with various components from both PBE and HSE06 methods is similar (Fang et al., 2019). Therefore, the band gap underestimated by the DFT method has no effect on the trend of band gap variation of materials with various components. In addition, the HSE06 method is not suitable for calculating the band structure of $NaSbS_2$ with minor Ga doping. The trend of band gap variation of $NaSb_{1-x}Ga_xS_2$ is predicted by the DFT method in the present study. In $NaSbS_2$, the VBM is mainly dominated by the S-3p orbitals, while the CBM are contributed from the Sb-5p and S-3p orbitals. It is noted that Na has no contribution to the band edges. Moreover, the flat CBM and slope VBM indicate that the effective mass difference between electron and hole is significant, and $NaSbS_2$ is actually a p-type semiconductor.

Fig. 4 shows the band structure and density of states of $NaSb_{1-x}Ga_xS_2$ with different Ga concentrations. It can be seen from Fig. 4 that all the Ga-doped compounds are direct band gap semiconductors at the τ point. The results indicate that the transition from an indirect-to-direct band gap for $NaSbS_2$ can be realized by doping Ga. The flat CBM and VBM imply that the large effective masses for electron and hole will exist, which is not preferred for thin-film solar cell applications. The contribution of the Ga-4 s and Ga-4p orbitals is negligible for the band edges when the doping Ga concentration is low. Therefore, it is speculated for $NaSb_{1-x}Ga_xS_2$ with × = 0.03125–0. 125 that the small band gap variation may be caused by local structural changes. However, the CBM of $NaSb_{0.75}Ga_{0.25}S_2$ is derived from the Sb-5p, Ga-4 s, and S-3p orbitals, and the VBM is still from the S-3p orbitals. It is clear that the intervention of the Ga-4 s orbitals is related to the larger bandgap of $NaSb_{0.75}Ga_{0.25}S_2$. The band gap variation trend for $NaSbS_2$ with various components is displayed in Fig. 5. An enlarged band gap is found for $NaSbS_2$ when the doping Ga concentration increases. There is no obvious effect on the band gap of $NaSbS_2$ when the doping Ga concentration is less than 10 %. The band gap increases by 0.5 eV from $NaSbS_2$ to $NaSb_{0.75}Ga_{0.25}S_2$. The results show that it is indeed an effective strategy to achieve the transition from an indirect to direct band gap for $NaSbS_2$ with maintaining the initial electronic properties through the low concentration of Ga doping.

The effect of parity-forbidden transition for halide perovskites was systematically reported in the previous theoretical study (Meng et al., 2017). For example, $CsBI_3$ (B = Ge, Sn, Pb) with a direct band gap shows no parity-forbidden transi-

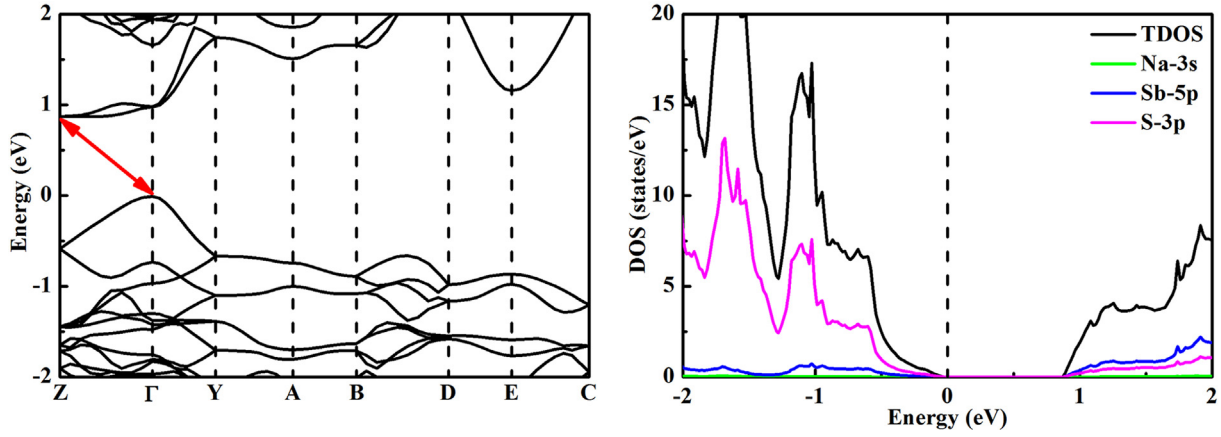

Fig. 3 Band structure (left) and density of states (right) of $NaSbS_2$.

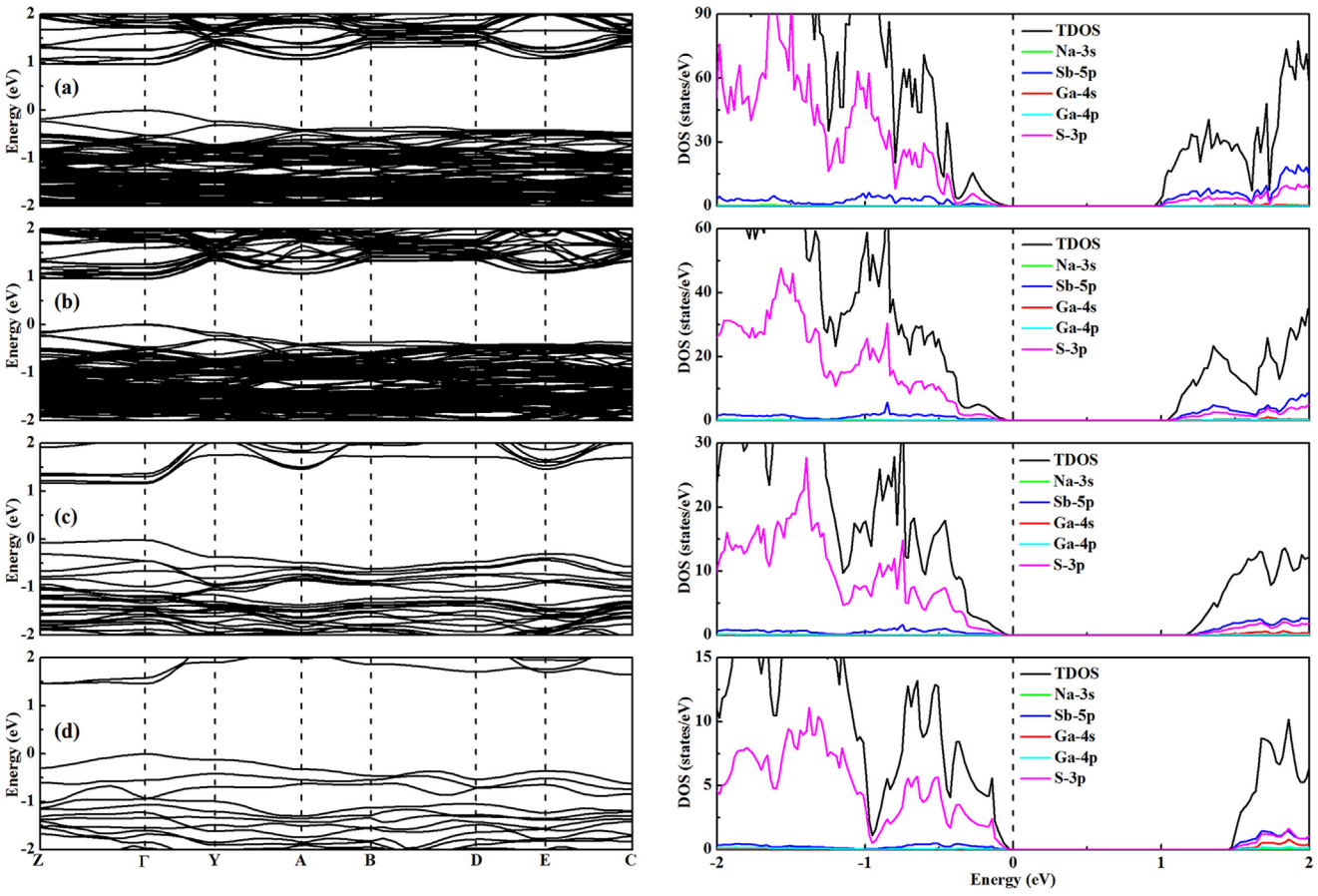

Fig. 4 Band structure (left) and density of states (right) of $NaSb_{1-x}Ga_xS_2$ with different Ga concentrations: (a) 3.125%, (b) 6.25%, (c) 12.5%, and (d) 25%.

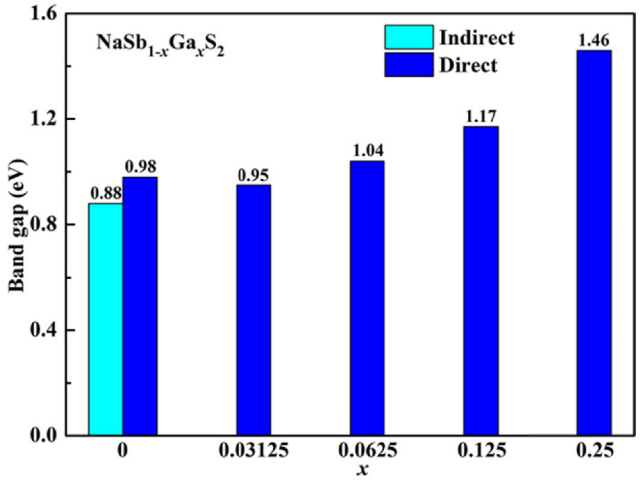

Fig. 5 The band gap value of $NaSb_{1-x}Ga_xS_2$ as a function of Ga concentration.

tions at the R point. The transition probability between the VBM and CBM can be revealed by calculating the transition dipole moment (TDM). The computed TDM values of $NaSbS_2$ and $NaSb_{0.75}Ga_{0.25}S_2$ at various k points are shown in Fig. 6(a-b). It is clear that the calculated TDM value is zero at the τ point, which indicates that the transition is forbidden at the τ point. The direct allowed band gap of $NaSbS_2$ at the Z point is 0.48 eV larger than the direct forbidden band gap at the τ point. It is observed from Fig. 6(b) that the transition is allowed at the τ point for $NaSb_{0.75}Ga_{0.25}S_2$. Fig. 6(c) shows the calculated TDM value of $NaSb_{1-x}Ga_xS_2$ at the τ point as a function of Ga concentration. The results suggest that with the increase of low Ga content, the TDM value is small and increases slowly. The weak transition is allowed for $NaSb_{1-x}Ga_xS_2$ when it has a direct band gap at the τ point. The strong transition will be allowed for $NaSb_{0.75}Ga_{0.25}S_2$ with a large TDM value. However, the band gap is greatly increased by doping high concentration of Ga. Therefore, the doping Ga concentration needs to be controlled reasonably for $NaSbS_2$ in order to balance the values between TDM and band gap.

3.3. Optical properties

The optical properties α(ω) can be calculated by the real $\varepsilon_1(\omega)$ and imaginary $\varepsilon_2(\omega)$ parts of dielectric function ε(ω). Two parameters $\varepsilon_1(\omega)$ and $\varepsilon_2(\omega)$ are related to each other through Kramer-Kronig relation (Gajdoš et al., 2006). The calculated optical absorption spectra of $NaSb_{1-x}Ga_xS_2$ is presented in Fig. 7. The optical absorption is directly related to the band gap of the compound. The low concentration Ga-doped $NaSbS_2$ and pure $NaSbS_2$ show similar optical properties. The light absorption capacity of $NaSb_{0.875}Ga_{0.125}S_2$ is slightly reduced compared to pure $NaSbS_2$. The optical absorption

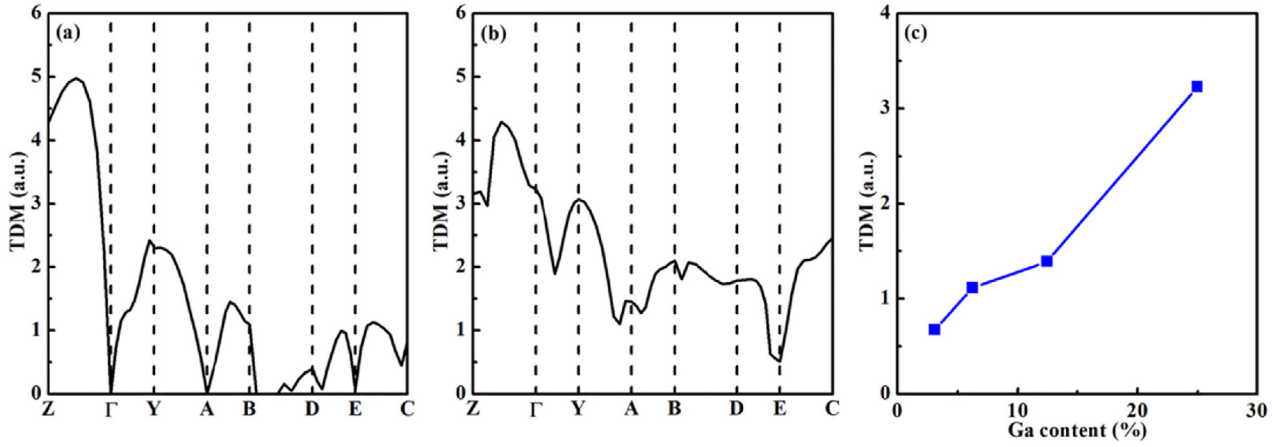

Fig. 6 The TDM values of (a) $NaSbS_2$ and (b) $NaSb_{0.75}Ga_{0.25}S_2$ at various k points and (c) $NaSb_{1-x}Ga_xS_2$ at the τ point.

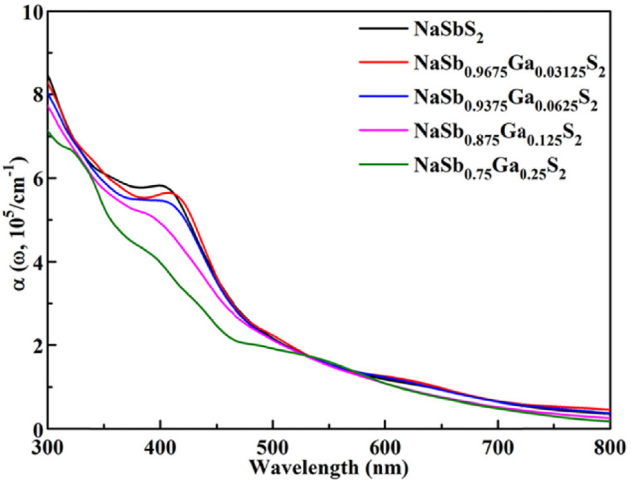

Fig. 7 Computed optical absorption spectra of $NaSb_{1-x}Ga_xS_2$ with × = 0–0.25.

coefficient of $NaSb_{0.75}Ga_{0.25}S_2$ is lower than that of $NaSbS_2$ in the range of 300–500 nm, which is attributed to the larger band gap. The relationship between the optical properties and band-gap is inversely proportional, and the decrease of optical absorption is mainly located near 400 nm. Therefore, it is expected to improve the photovoltaic performance of $NaSbS_2$ with the help of the low concentration Ga doping.

4. Conclusion

In summary, the present work is performed to discover the impact of Ga doping on the structure, electronic, and optical properties of $NaSbS_2$. $NaSbS_2$ is an indirect band gap compound, and the energy difference between the indirect and direct band gaps is small. The forbidden transition is found for the fundamental direct bandgap of $NaSbS_2$. The negative ΔH values indicate that the $NaSb_{1-x}Ga_xS_2$ alloys can be synthesized and confirm their thermodynamic stability. An indirect-to-direct band gap transition is discovered from $NaSbS_2$ to $NaSb_{1-x}Ga_xS_2$. The effect of low concentration Ga doping (less than10 %) is negligible for the electronic and optical properties of $NaSbS_2$. However, the band gap of $NaSbS_2$ is greatly increased when the concentration of Ga doping is high. Furthermore, the weak transition of the fundamental direct bandgap is allowed for $NaSb_{1-x}Ga_xS_2$. Therefore, this finding makes $NaSbS_2$ more favorable for solar cells. Our study will contribute to improve the efficiency of based-$NaSbS_2$ materials in the future.

Declaration of competing interest

The authors declare that they have no known competing financial interests or personal relationships that could have appeared to influence the work reported in this paper.

Acknowledgments

This work was supported by the Open Project of Fujian Key Laboratory of Functional Marine Sensing Materials (No. MJUKF-FMSM202012).

References

Adhikary, A., Yaghoobnejad Asl, H., Sandineni, P., Balijapelly, S., Mohapatra, S., Khatua, S., Konar, S., Gerasimchuk, N., Chernatynskiy, A.V., Choudhury, A., 2020. Unusual atmospheric water trapping and water induced reversible restacking of 2D Gallium Sulfide layers in $NaGaS_2$ formed by supertetrahedral building unit. Chem. Mater. 32, 5589–5603.

Aragaw, B.A., Sun, J., Singh, D.J., Lee, M.-W., 2017. Ion exchange-prepared $NaSbSe_2$ nanocrystals: electronic structure and photovoltaic properties of a new solar absorber material. RSC Adv. 7, 45470–45477.

Bazakutsa, V.A., Gnidash, N.I., Kul'chitskaya, A.K., Salov, A.V., 1975. Photoelectric and optical properties of thin films of ternary chalcogenides of the form $MeISbX_2VI$. Sov. Phys. J. 18, 472–475.

Blöchl, P.E., 1994. Projector augmented-wave method. Phys. Rev. B 50, 17953–17979.

Bouchenafa, M., Sidoumou, M., Halit, M., Benmakhlouf, A., Bouhemadou, A., Maabed, S., Bentabet, A., Bin-Omran, S., 2018. Theoretical investigation of the structural, elastic, electronic and optical properties of the ternary indium sulfide layered structures $AInS_2$ (A = K, Rb and Cs). Solid State Sci. 76, 74–84.

Choi, Y.C., Yeom, E.J., Ahn, T.K., Seok, S.I., 2015. $CuSbS_2$-sensitized inorganic-organic heterojunction solar cells fabricated using a metal-Thiourea complex solution. Angew. Chem. Int. Ed. 54, 4005–4009.

Dai, C.-M., Xu, P., Huang, M., Cai, Z.-H., Han, D., Wu, Y., Chen, S., 2019. $NaSbSe_2$ as a promising light-absorber semiconductor in solar cells: first-principles insights. APL Mater. 7, 081122.

Eisenmann, B., Hofmann, A., 1991. Crystal structure of potassium phyllo-dithioindate(III), $KInS_2$. Z Krist. Cryst. Mater. 195, 318–319.

Fang, Z., Shang, M., Hou, X., Zheng, Y., Du, Z., Yang, Z., Chou, K.-C., Yang, W., Wang, Z.L., Yang, Y., 2019. Bandgap alignment of α-$CsPbI_3$ perovskites with synergistically enhanced stability and optical performance via B-site minor doping. Nano Energy 61, 389–396.

Fukuzaki, K., Kohiki, S., Matsushima, S., Oku, M., Hideshima, T., Watanabe, T., Takahashi, S., Shimooka, H., 2000. Preparation and characterization of $NaInO_2$ and $NaInS_2$. J. Mater. Chem. 10, 779–782.

Gajdoš, M., Hummer, K., Kresse, G., Furthmüller, J., Bechstedt, F., 2006. Linear optical properties in the projector-augmented wave methodology. Phys. Rev. B 73, 045112.

Ho, Y.-R., Lee, M.-W., 2013. $AgSbS_2$ semiconductor-sensitized solar cells. Electrochem. Commun. 26, 48–51.

Hoppe, R., Lidecke, W., Frorath, F.-C., 1961. Zur Kenntnis von $NaInS_2$ und $NaInSe_2$. Z. Anorg. Allg. Chem. 309, 49–54.

Hossain, M.M., Ali, M.A., Uddin, M.M., Hossain, M.A., Rasadujjaman, M., Naqib, S.H., Nagao, M., Watauchi, S., Tanaka, I., 2021a. Influence of Se doping on recently synthesized $NaInS_{2-x}Se_x$ solid solutions for potential thermo-mechanical applications studied via first-principles method. Mater. Today Commun. 26, 101988.

Hossain, M.M., Hossain, M.A., Moon, S.A., Ali, M.A., Uddin, M.M., Naqib, S.H., Islam, A.K.M.A., Nagao, M., Watauchi, S., Tanaka, I., 2021b. $NaInX_2$ (X = S, Se) layered materials for energy harvesting applications: first-principles insights into optoelectronic and thermoelectric properties. J. Mater. Sci.: Mater. Electron. 32, 3878–3893.

Huang, P.-C., Yang, W.-C., Lee, M.-W., 2013. $AgBiS_2$ semiconductor-sensitized solar cells. J. Phys. Chem. C 117, 18308–18314.

Kang, Y., Youn, Y., Han, S., Park, J., Oh, C.-S., 2019. Computational screening of indirect-gap semiconductors for potential photovoltaic absorbers. Chem. Mater. 31, 4072–4080.

Khare, I.S., Szymanski, N.J., Gall, D., Irving, R.E., 2020. Electronic, optical, and thermoelectric properties of sodium pnictogen chalcogenides: a first principles study. Comput. Mater. Sci. 183, 109818.

Klepov, V.V., Berseneva, A.A., Pace, K.A., Kocevski, V., Sun, M., Qiu, P., Wang, H., Chen, F., Besmann, T.M., zur Loye, H.C., 2020. $NaGaS_2$: an elusive layered compound with dynamic water absorption and wide-ranging ion-exchange properties. Angew. Chem. Int. Ed. 59, 10836–10841.

Kresse, G., Furthmüller, J., 1996. Efficiency of ab-initio total energy calculations for metals and semiconductors using a plane-wave basis set. Comput. Mater. Sci. 6, 15–50.

Leung, W.W.W., Savory, C.N., Palgrave, R.G., Scanlon, D.O., 2019. An experimental and theoretical study into $NaSbS_2$ as an emerging solar absorber. J. Mater. Chem. C 7, 2059–2067.

Liu, D., Huang, S., Wang, X., Sa, R., 2021. (Li, Na)Sb_S2 as a promising solar absorber material: a theoretical investigation. Spectrochim. Acta. A Mol Biomol. Spectrosc. 250, 119389.

Mahmoud, M.M.A., Joubert, D.P., Molepo, M.P., 2019. Structural, stability and thermoelectric properties for the monoclinic phase of $NaSbS_2$ and $NaSbSe_2$: a theoretical investigation. Eur. Phys. J. B 92, 214.

Meng, W., Wang, X., Xiao, Z., Wang, J., Mitzi, D.B., Yan, Y., 2017. Parity-forbidden transitions and their impact on the optical absorption properties of lead-free metal halide perovskites and double perovskites. J. Phys. Chem. Lett. 8, 2999–3007.

Olivier-Fourcade, J., Philippot, E., Maurin, M., 1978. Structure des composés $NaSbS_2$α et $NaSbS_2$β. Etude de l'influence de la paire electronique E de l'antimonine III dans Ia transition $NaSbS_2$α → $NaSbS_2$β. Z. Anorg. Allg. Chem. 446, 159–168.

Perdew, J.P., Burke, K., Ernzerhof, M., 1996. Generalized gradient approximation made simple. Phys. Rev. Lett. 77, 3865–3868.

Rahayu, S.U., Chou, C.-L., Suriyawong, N., Aragaw, B.A., Shi, J.-B., Lee, M.-W., 2016. Sodium antimony sulfide ($NaSbS_2$): Turning an unexpected impurity into a promising, environmentally friendly novel solar absorber material. APL Mater. 4, 116103.

Rosales, B.A., White, M.A., Vela, J., 2018. Solution-grown sodium bismuth dichalcogenides: toward earth-abundant, biocompatible semiconductors. J. Am. Chem. Soc. 140, 3736–3742.

Sa, R., Zhang, Q., Yang, Y., Liu, D., 2022. Bandgap engineering of $Na_{1-x}Ag_xSbS_2$ alloys for photovoltaic applications. Mater. Res. Bull. 152, 111862.

Sun, J., Singh, D.J., 2017. Electronic properties, screening, and efficient carrier transport in $NaSbS_2$. Phys. Rev. Applied 7, 024015.

Takahashi, N., Ito, H., Miura, A., Rosero-Navarro, N.C., Goto, Y., Mizuguchi, Y., Moriyoshi, C., Kuroiwa, Y., Nagao, M., Watauchi, S., Tanaka, I., Tadanaga, K., 2018. Synthesis, crystal structure and optical absorption of $NaInS_{2-x}Se_x$. J. Alloys Compd. 750, 409–413.

Welch, A.W., Baranowski, L.L., Zawadzki, P., Lany, S., Wolden, C. A., Zakutayev, A., 2015. $CuSbSe_2$ photovoltaic devices with 3% efficiency. Appl. Phys. Express 8, 082301.

Xia, Z., Yu, F.-X., Lu, S.-C., Xue, D.-J., He, Y.-S., Yang, B., Wang, C., Ding, R.-Q., Zhong, J., Tang, J., 2017. Synthesis and characterization of $NaSbS_2$ thin film for potential photodetector and photovoltaic application. Chin. Chem. Lett. 28, 881–887.

Yang, C., Wang, Z., Wu, Y., Lv, Y., Zhou, B., Zhang, W.-H., 2019. Synthesis, characterization, and photodetector application of alkali metal bismuth chalcogenide nanocrystals. ACS Appl. Energy Mater. 2, 182–186.

Yun, Y., Xie, W., Yang, Z., Li, G., Pan, S., 2022. Na^+/Ag^+ substitution induced birefringence enhancement from $AgGaS_2$ to $NaGaS_2$. J. Alloys Compd. 896, 163093.

Zeng, H.-Y., Zheng, F.-K., Chen, R.-P., Dong, Z.-C., Guo, G.-C., Huang, J.-S., 2007. Reactive flux syntheses, crystal structures and band gaps of $AInS_2$ (A = Rb, Cs). J. Alloys Compd. 432, 69–73.

Zhang, X., Huang, M., Xu, P., Dai, C.-M., Cai, Z.-H., Han, D., Chen, S., 2019. Earth-abundant photovoltaic semiconductor $NaSbS_2$ in the rocksalt-derived structure: a first-principles study. Prog. Nat. Sci-Mater. 29, 322–328.